Electric Power Systems Research 212 (2022) 108462

Contents lists available at ScienceDirect

Electric Power Systems Research

journal homepage: www.elsevier.com/locate/epsr

Stochastic operation of energy constrained microgrids considering battery degradation☆

Per Aaslid [a,b,*], Magnus Korpås [b], Michael M. Belsnes [a], Olav B. Fosso [b]

[a] Department of Energy Systems, SINTEF Energy Research, Trondheim, Norway
[b] Department of Electrical Power Engineering, Norwegian University of Science and Technology, Trondheim, Norway

ARTICLE INFO

Keywords:
Energy management
Electric energy storage
Multi-stage stochastic programming
Battery degradation

ABSTRACT

Power systems with high penetration of variable renewable generation are vulnerable to periods with low generation. An alternative to retain high dispatchable generation capacity is electric energy storage that enables utilization of surplus power, where the electric energy storage contributes to the security of supply. Such systems can be considered as energy-constrained, and the operation of the electric energy storage must balance the minimization of the current operating costs against the risk of not being able to meet the future demand. Safe and efficient operation requires stochastic methods with sufficient foresight. Operation dependent storage degradation is a complicating factor. This paper proposes a linear approximation of battery state-of-charge degradation and implements it in a stochastic dual dynamic programming based energy-management model in combination with cycling degradation. The long-term implications of degradation modeling in the daily operation are studied for a small Norwegian microgrid with variable renewable power generation and limited dispatchable generation capacity as well as battery and hydrogen storage to balance supply and demand. Our results show that the proposed strategy can prolong the expected battery lifetime by more than four years compared to the naive stochastic strategy but may cause increased degradation for other system resources.

1. Introduction

Electricity systems with high penetration of variable renewable energy sources (VRESs) rely on sufficient dispatchable generation capacity to meet the peak demand in periods with low VRES generation. An alternative to dispatchable thermal generation capacity is to utilize EES flexibility. A challenge with EES is that the current decision also affects the energy content and the capability of providing capacity in the future. The decisions here and now must be taken while accounting for future power generation and load under uncertainty, and needs to balance the risk of generation curtailment versus the risk of not being able to meet the demand. The operation of EES in these situations can be seen as a precaution or arbitrage against extreme prices [1,2]. Moreover, these systems require significant VRES overcapacity and will also be exposed to lasting periods with excess energy resulting in generation curtailment [3]. The EESs must be operated to balance short-term variations in generation and demand, and also store energy for potential future energy deficit.

Different EES technologies have complementary properties with respect to power and energy scalability. Lithium-ion batteries have gained high attention both in the research community as well as for power system applications due to their ability to deliver and absorb very high power almost instantaneously with very high efficiency. They also have a relatively high energy to weight ratio compared to similar battery technologies. A key factor of large scale VRES integration is long-duration energy storage [4]. Batteries are expensive to scale up with respect to energy compared to hydrogen, which can be stored in large tanks and scaled up at a relatively low cost. However, the cost of fuel cells and electrolyzers are still very high, and the round-trip efficiency is poor compared to batteries [5].

Unlike traditional thermal power generators where the marginal operating cost is well defined based on fuel and emission costs, VRESs have marginal operating cost close to zero. However, the expected lifetime of the power system components, such as the EESs, are influenced by their operational pattern. Degradation characteristics differ for batteries and hydrogen systems. The aging of hydrogen fuel cells are largely affected by start, stop and rapid ramping. However, the degradation has often been studied for vehicles that exhibit several cycles each hour [6], while a grid connected fuel cell will operate with less frequent cycling. Moreover, degradation of fuel cells can also be related to dry membranes caused by limited operation, and modest operation

☆ This work has been funded by the Norwegian Research Council, Norway under grant number 272398.
* Corresponding author at: Department of Energy Systems, SINTEF Energy Research, Trondheim, Norway.
E-mail address: per.aaslid@sintef.no (P. Aaslid).

https://doi.org/10.1016/j.epsr.2022.108462
Received 30 September 2021; Received in revised form 13 April 2022; Accepted 2 July 2022
Available online 27 July 2022

can extend the expected lifetime compared to low operation [7]. The degradation cost of the hydrogen system has therefore been neglected.

The degradation of lithium-ion batteries is closely related to operating conditions like charge/discharge power, depth-of-discharge (DOD), SOC, temperature, and ampere throughput [8]. Energy management of VRES typically involves daily cycles, and the battery will rarely operate close to its maximum power capabilities. Moreover, the battery temperature will be controlled to ensure optimal operating conditions and minimal degradation. Whereas balancing the short-term fluctuation causes degradation due to DOD, long-term storage increases the SOC degradation. This paper will therefore consider degradation caused by DOD and SOC.

The aging is therefore influenced by the operational pattern, and the optimal power dispatch largely depends on the battery's aging model [9]. Previous studies of microgrid (MG) economic dispatch often neglect the cost associated with degradation [10,11]. Single factor models, considering degradation either as a function of power, SOC, DOD, or ampere hour throughput, are also widely adopted [9]. For example, Refs. [12–15] assume the degradation is proportional with energy throughput. More sophisticated models capture non-linear effects, either as a single factor model [16] or combined models [17,18].

However, previous studies mainly focus on daily battery cycling under variable photovoltaic (PV) generation with deterministic models [9,16,17]. This paper also considers the effect of lasting generation surplus and deficit with respect to how the battery and hydrogen storage are operated. To account for the uncertainty in generation from VRES, which is crucial for energy constrained systems [19], a multi-stage stochastic formulation is implemented. Moreover, the expected implication on the battery lifetime is considered using actual data for a real MG over a whole year.

Non-linear models are often computationally intensive, especially for large-scale systems and stochastic problems. Convex and linear problem formulations reduce the computational burden, and enable utilization of decomposition techniques such as dual decomposition. Ref. [20] proposes a piece-wise linear relaxation of the non-linear DOD degradation, and shows that a cost reduction can be achieved by considering the cyclic degradation in the market clearing of a battery. However, linear approximation of the non-linear SOC degradation has gained less attention.

This paper proposes a piece-wise linear approximation of the battery SOC degradation effect, and demonstrates it in combination with linear DOD degradation [20] on a real MG from the EU project REMOTE [21,22]. The system is operating islanded, and is energy constrained since the backup generator is too small to cover the peak demand and the EES must be operated to prevent load shedding in extreme situations. The optimal operation is considered using rolling horizon [23] and stochastic dual dynamic programming (SDDP) [24]. The system is simulated for a whole year with rolling horizon using real observations from the MG and scenarios generated from historical weather forecasts. Infinite horizon is embedded using cyclic Markov chains [25], and the implication of including battery degradation will be studied with respect to the costs, VRES and EES utilization as well as expected battery lifetime.

The contributions of this paper can be summarized as: (*i*) a linear battery SOC degradation formulation, (*iii*) a multi-stage stochastic energy management formulation including both battery DOD and SOC degradation, and (*iii*) an analysis of a full year operation of an actual MG using the proposed formulation to valuate the importance of considering battery degradation in a life cycle perspective.

The remainder of the paper is organized as follows: Section 2 describes the rolling horizon simulation method as well as the SDDP algorithm, and derives the linear power system model including the SOC degradation model; Section 3 presents how the proposed method is implemented and the numerical values of the cases; Section 4 shows and discusses the results; and Section 5 draws the conclusions and suggests future work.

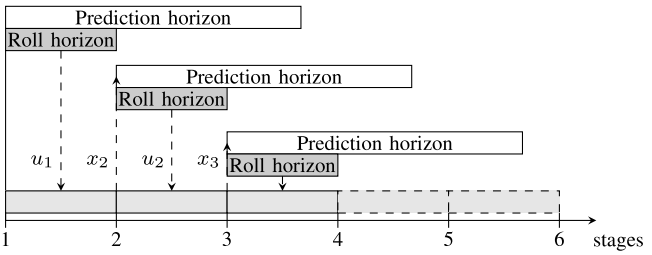

Fig. 1. Rolling horizon optimization.

2. Method

This section presents the rolling horizon stochastic energy-management model where the goal is to find the optimal stage-wise control decisions u_s at each stage s for the in-going state x_s and the stage-wise uncertainty ω_s.

2.1. Rolling horizon simulation

Generation forecasts are based on weather forecasts issued with fixed intervals, and the stochastic model is trained each time a new forecast is available for the prediction horizon as illustrated in Fig. 1. The actual generation and demand is observed and evaluated for the roll horizon interval using the trained stochastic model yielding the optimal control u_s that is implemented. Finally, the optimization horizon is moved forward and the procedure is repeated using the end state x_{s+1} from previous optimization as the initial value.

2.2. Multi-stage stochastic programming

This paper considers multi-stage stochastic programming (MSSP) for solving the proposed energy management problem. MSSP captures that energy management is a sequential decision making process and recognizes that decisions can be updated stage-wise as uncertainty is revealed. The MSSP formulation in (1a)–(1c) is divided into several stages s, each representing a discrete moment in time. The goal is to minimize the current and future operating costs. State variables x_s represent variables connected across stages, such as EES SOC. Control variables u_s are decisions, both implicit and explicit, and must be within the technical limitations of the system given by the set of admissible controls (1c). The state transition function (1b) describes the relation between the state variables across stages. The random variable ω_s represents the uncertainty in demand and VRES generation.

$$\min_{u_t}\Bigg\{C_1(x_1,u_1,\omega_1)+\mathop{\mathbb{E}}_{\omega_2|\omega_1}\Bigg[\min_{u_2}\Big(C_2(x_2,u_2,\omega_2)+\cdots + \mathop{\mathbb{E}}_{\omega_S|\omega_{S-1},\ldots,\omega_2}\Big[\min_{u_S}\big(C_S(x_S,u_S,\omega_S)\big)\Big]\Big)\Bigg]\Bigg\} \tag{1a}$$

$$\text{s.t.}\quad x_{s+1}=T_s(x_s,u_s,\omega_s) \tag{1b}$$

$$u_s\in U_s(x_s,\omega_s) \tag{1c}$$

Generation from solar and wind power are correlated and has significant auto-correlation. However, the auto-correlation is partially captured by the stage-wise scenarios that can span several hours. By assuming the random variable is stage-wise independent and has a discrete set of realizations for each stage, the problem can be formulated on extended form. Instead of solving the intractable extended problem, SDDP [24] decomposes the problem into sub-problems for each stage $s\in S$ and realization of the random variable $\omega_s\in\Omega_s$ as shown in (2a)–(2e). The algorithm is divided into two phases: forward pass and backward recursion. The forward pass samples a random variable for

each stage and solves the sequence of sub-problems using the outgoing state of stage s as the in-going state to stage $s+1$. When the final stage is reached, the backward recursion starts by solving the final stage for all the random variables. From convexity, the dual variables λ_s of the state variable x_s (2b) can be used to generate a linear cutting plane (2e) that acts as a lower bound for the previous stage problem, and the procedure is repeated all the way back to the first stage. The whole procedure is repeated, adding new cuts for each iteration k, until the convergence criteria is met [24,25] and it has been shown that the algorithm under certain conditions will converge [26].

$$\min_{u_s, x_s, x_{s+1}, \theta_s} C_s(x_s, u_s, \omega_s) + \theta_s \tag{2a}$$

$$\text{s.t. } x_s = \bar{x_s}, \quad [\lambda_s] \tag{2b}$$

$$x_{s+1} = T_s(x_s, u_s, \omega_s) \tag{2c}$$

$$u_s \in U_s(x_s, \omega_s) \tag{2d}$$

$$\theta_s \geq \alpha_s^k + \beta_s^k x_{s+1}, \quad k \in \{1, 2, \dots, K\} \tag{2e}$$

2.3. Power system model

Each stage-wise problem in (1a)–(1c) comprises a power system model with multiple timesteps t. The power system model including the battery degradation model will be expressed using the following sets and indices:

- $t \in \mathcal{T}_s$: Time index t and the set of time steps $\mathcal{T}_s$ from stage s.
- $g \in \mathcal{G}$: Generator g and the set of dispatchable generators $\mathcal{G}$.
- $r \in \mathcal{R}$: VRES r and the set of VRESs $\mathcal{R}$.
- $d \in \mathcal{D}$: Consumer d and the set of consumers $\mathcal{D}$.
- $e \in \mathcal{E}$: EES e and the set of EESs $\mathcal{E}$.
- $k_\delta \in \mathcal{K}_\delta$: Battery cycling segment k_δ in the set of segments $\mathcal{K}_\delta$.
- $k_\sigma^{up} \in \mathcal{K}_\sigma^{up} / k_\sigma^{dn} \in \mathcal{K}_\sigma^{up}$: Battery SOC segment $k_\sigma^{up}/k_\sigma^{dn}$ direction up/down in the set of segments $\mathcal{K}_\sigma^{up}/\mathcal{K}_\sigma^{up}$ respectively.

The following parameters have been used:

- ΔT_t: Timestep t step length.
- PG_g^{max}: Generator g maximum power dispatch.
- C_g: Generator g marginal operating cost.
- $PR_{r,t}^{max}$: VRES r maximum power at time t.
- $PD_{d,t}$: Demand of consumer d at time t.
- C_d: Consumer d marginal load shedding cost.
- SOC_e^{min}/SOC_e^{max}: EES e minimum and maximum SOC.
- PS_e^c/PS_e^d: EES e maximum charge/discharge power.
- C_{e,k_δ}: EES e DOD marginal degradation cost segment k.
- SOC_e^{ref}: EES e SOC degradation reference value.
- $C_{e,k_\sigma}^{up}/C_{e,k_\sigma}^{dn}$: EES e SOC marginal degradation cost up/down segment $k_\sigma^{up}/k_\sigma^{dn}$.
- η_e^c/η_e^d: EES e charge/discharge efficiency.
- R: Battery replacement cost.

The functions and variables are:

- $p_{g,t}$: Generator g power dispatch at time t.
- $p_{g,t}$: VRES r power dispatch at time t.
- $p_{d,t}$: Consumer d demand at time t.
- $pls_{d,t}$: Consumer d load shedding at time t.
- $ps_{e,t(,k_\delta)}^c/ps_{e,t(,k_\delta)}^d$: EES e power charge/discharge DOD (segment k_δ) at time t.
- soc_{e,t,k_δ}: EES e SOC DOD segment k_δ at time t.
- $soc_{e,t,k_\sigma}^{up}/soc_{e,t,k_\sigma}^{dn}$: EES e SOC degradation segment $k_\sigma^{up}/k_\sigma^{dn}$ above/below reference value at time t.
- δ_t: Unitless EES cycle depth at time t.
- σ_t: Unitless EES SOC at time t.
- σ^{ref}: Unitless EES reference SOC.
- $f_\delta(\delta_t)$: Incremental battery fade as a function of cycle depth δ_t at time t.
- $f_\sigma(\sigma_t)$: Incremental battery fade as a function of SOC σ_t at time t.

The resulting model is summarized in (3)–(13). The objective is to minimize the dispatchable generation costs, load shedding, and EES degradation associated with both DOD and SOC (3). The total power injections and withdrawals must balance at all time steps (4). The generation, both dispatchable and VRES, must respect the maximum generation (5) and (6). Demand that cannot be met, causes load shedding (7). The battery charge/discharge must respect the maximum limits, both per segment (8) and (9) and the sum of the segments (10) and (11). The EES energy balance is expressed per segment (12), where the segments are divided into equal sizes (13).

$$\min \sum_{t \in \mathcal{T}} \left[\sum_{g \in \mathcal{G}} C_g p_{g,t} + \sum_{d \in \mathcal{D}} C_d pls_{d,t} + \sum_{e \in \mathcal{E}} \sum_{j \in \mathcal{J}} C_{e,k_\delta} ps_{e,t,k_\delta}^d + \sum_{e \in \mathcal{E}} \left(\sum_{k_\sigma \in \mathcal{K}_\sigma^{up}} C_{e,k_\sigma}^{up} soc_{e,t,k_\sigma}^{up} + \sum_{k_\sigma \in \mathcal{K}_\sigma^{dn}} C_{e,k_\sigma}^{dn} soc_{e,t,k_\sigma}^{dn} \right) \right] \tag{3}$$

subject to

$$\sum_{g \in \mathcal{G}} p_{g,t} + \sum_{r \in \mathcal{R}} p_{r,t} + \sum_{e \in \mathcal{E}} ps_{e,t}^d = \sum_{d \in \mathcal{D}} p_{d,t} + \sum_{e \in \mathcal{E}} ps_{e,t}^c \tag{4}$$

$$0 \leq p_{g,t} \leq PG_g^{max} \tag{5}$$

$$0 \leq p_{r,t} \leq PR_{r,t}^{max} \tag{6}$$

$$p_{d,t} = PD_{d,t} - pls_{d,t} \tag{7}$$

$$0 \leq ps_{e,t,k_\delta}^c \leq PS_e^c \tag{8}$$

$$0 \leq ps_{e,t,k_\delta}^d \leq PS_e^d \tag{9}$$

$$ps_{e,t}^c = \sum_{j \in \mathcal{J}} ps_{e,t,k_\delta}^c \leq PS_e^c \tag{10}$$

$$ps_{e,t}^d = \sum_{j \in \mathcal{J}} ps_{e,t,k_\delta}^d \leq PS_e^d \tag{11}$$

$$soc_{e,t,k_\delta} = soc_{e,t-1,k_\delta} + \Delta T_t \left(\eta_e^c ps_{e,t,k_\delta}^c - \frac{1}{\eta_e^d} ps_{e,t,k_\delta}^d \right) \tag{12}$$

$$0 \leq soc_{e,t,k_\delta} \leq \frac{1}{|\mathcal{K}_\delta|} (SOC_e^{max} - SOC_e^{min}) \tag{13}$$

Note that restrictions to prevent simultaneous charging and discharging have not been included since it requires integer variables or non-linear modeling. This assumption implies that dumping of energy from the battery is accepted. This is not a problem when the VRES generation can be curtailed at no cost. However, by introducing SOC degradation cost, situations where dumping of energy is beneficial might arise. Moreover, minimum power for the thermal generator and the hydrogen system has not been considered since it would require binary variables that is not supported by standard SDDP. As a consequence, the flexibility of the diesel generator and the hydrogen system is overestimated and the battery cycling need might be underestimated. This limitation can be overcome by using SDDiP [27], but would increase the computational burden significantly.

The state x_s comprises the initial SOC variable soc_{e,t,k_δ} at each stage, and the final SOC variable at the outgoing state x_{s+1}. The random variable ω comprises the renewable generation $PR_{r,t}^{max}$ and the demand $PD_{d,t}$ for all the steps in the stage. The remaining variables are decisions u_s, either explicit or implicit.

2.4. EES degradation model

Experimental results show that the degradation rate of lithium-ion batteries increases with increasing DOD. Moreover, the degradation rate is also higher for high SOC [28,29], but very low SOC will also cause high degradation [30–33].

The proposed model assumes the degradation due to DOD and SOC are decoupled. For an arbitrary convex DOD capacity fade function $f_\delta(\delta_t)$, the EES SOC is divided into equally sized segments K_δ yielding cost coefficients $C_{\delta k}$ (14) [20].

$$C_{\delta k} = \frac{R}{\eta^d SOC^{max}} |\mathcal{K}_\delta| \left[f_\delta\left(\frac{k}{|\mathcal{K}_\delta|}\right) - f_\delta\left(\frac{k-1}{|\mathcal{K}_\delta|}\right)\right], k \in \mathcal{K}_\delta \tag{14}$$

Each energy level soc_t and charge/discharge ps_t^c/ps_t^d is divided into K_δ segments. Since the marginal cost curve is convex, the cheapest available segment will always be discharged, and the suggested method will therefore count cycles in a similar manner as the Rainflow counting algorithm [34].

The same principle can be used for modeling the SOC degradation. For an arbitrary convex SOC capacity fade function $f_\sigma(\sigma)$, as illustrated in Fig. 3, σ^{ref} represents the SOC level where the SOC degradation is lowest as shown in (15).

$$\sigma^{ref} = \underset{\sigma}{\operatorname{argmin}} f_\sigma(\sigma) \tag{15}$$

The incremental capacity fade as a function of SOC can be found by taking the derivative of $f_\sigma(\sigma)$ with respect to soc_t.

$$\frac{\partial f_\sigma(\sigma_t)}{\partial soc_t} = \frac{d f_\sigma(\sigma_t)}{d\sigma_t}\frac{\partial \sigma_t}{\partial soc_t} = \frac{1}{SOC^{max}}\frac{d f_\sigma(\sigma_t)}{d\sigma_t} \tag{16}$$

The $soc_{e,t}$ variable is divided into K_σ^{up} and K_σ^{dn} equally sized segments $soc_{e,t,k}^{up}$ and $soc_{e,t,k}^{dn}$ for up and down direction as illustrated by the orange and green segments in Fig. 3 respectively, and shown in (17)–(20). Therefore, $soc_{e,t,k}^{up}$ and $soc_{e,t,k}^{dn}$ represent the distance from the reference value in both directions.

$$\sum_{k\in\mathcal{K}_\sigma^{up}} soc_{e,t,k}^{up} \geq soc_{e,t} - SOC_e^{ref} \tag{17}$$

$$\sum_{k\in\mathcal{K}_\sigma^{dn}} soc_{e,t,k}^{dn} \geq SOC_e^{ref} - soc_{e,t} \tag{18}$$

$$0 \leq soc_{e,t,k}^{up} \leq \frac{1}{|\mathcal{K}_\sigma^{up}|}\left(SOC^{max} - SOC_e^{ref}\right) \tag{19}$$

$$0 \leq soc_{e,t,k}^{dn} \leq \frac{1}{|\mathcal{K}_\sigma^{dn}|} SOC_e^{ref} \tag{20}$$

Let $C_{\sigma,k}^{up}$ and $C_{\sigma,k}^{dn}$ denote the incremental aging cost with respect to each segment in either direction $soc_{e,t,k}^{up}$ and $soc_{e,t,k}^{dn}$, which can be interpreted as the segment slopes in Fig. 3. The resulting cost coefficients are expressed in (21) and (22).

$$C_{\sigma k}^{up} = \frac{R}{SOC^{max}}|\mathcal{K}_\sigma^{up}|\left[f_\sigma\left(\sigma^{ref} + \frac{k}{|\mathcal{K}_\sigma^{up}|}(1-\sigma^{ref})\right)\right.$$
$$\left. - f_\sigma\left(\sigma^{ref} + \frac{k-1}{|\mathcal{K}_\sigma^{up}|}(1-\sigma^{ref})\right)\right], k \in \mathcal{K}_\sigma^{up} \tag{21}$$

$$C_{\sigma k}^{dn} = \frac{R}{SOC^{max}}|\mathcal{K}_\sigma^{dn}|\left[f_\sigma\left(\sigma^{ref} - \frac{k}{|\mathcal{K}_\sigma^{dn}|}\sigma^{ref}\right)\right.$$
$$\left. - f_\sigma\left(\sigma^{ref} - \frac{k-1}{|\mathcal{K}_\sigma^{dn}|}\sigma^{ref}\right)\right], k \in \mathcal{K}_\sigma^{dn} \tag{22}$$

The cheapest segments will always be used first, and the correct segment will be used given a convex cost function. Non-convex cost functions should consider convex relaxation or mixed-integer programming to ensure global optimality but has not been considered in this paper.

3. Implementation and numerical values

The proposed method is implemented in Julia (1.4.2) with SDDP.jl (0.3.14) [35] and Gurobi (9.1). The models were trained with 50 SDDP iterations.

Table 1
Microgrid numerical values.

Description	Unit	Value
Wind turbine capacity	[kW]	135
Solar PV capacity	[kW]	86
Diesel generator capacity	[kW]	25/75
Diesel generation cost	[€/MWh]	100
Load shedding cost	[€/MWh]	5000

Table 2
Numerical values for microgrid EES.

Description	Unit	Lithium-ion	Hydrogen
Charge power	[kW]	500	55
Discharge power	[kW]	500	100
Size	[kWh]	500/1000	3300/–
Charge efficiency	[%]	96	64
Discharge efficiency	[%]	96	50
Replacement cost	[€/kWh]	100	NA

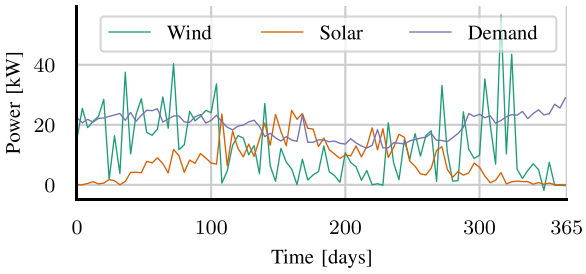

Fig. 2. Four day average generation and demand for the optimization period.

3.1. Microgrid

The model has been tested on the Rye microgrid in central Norway that is partly funded by the Horizon 2020 project REMOTE [21]. The MG comprises a few farms and houses, and is supplied by a wind turbine, solar PV, and a diesel generator that serves as backup in case of insufficient VRES generation. The system is equipped with battery and hydrogen storage to balance supply and demand [22]. Load shedding costs occur if the supply is unable to meet the demand. Numerical values for the MG are shown in Table 1, and the EES in Table 2. Note that the wind and diesel generator sizes in this case differs from the actual system. Fig. 2 shows the four day average VRES generation and demand for the whole period.

3.2. Battery degradation

This paper uses a quadratic DOD capacity fade function (23) [17,33]. The upper range of the SOC stress function (24) is exponential [36], while the lower part is defined to capture the potential collapse associated with operating at very low SOC [18,32]. Note that any convex fade function can be used.

$$f_\delta(\delta) = k_\delta\ \delta^2 \tag{23}$$

$$f_\sigma(\sigma) = \begin{cases} k_{\sigma 1} e^{k_{\sigma 2}(\sigma - \sigma^{ref})} & 0.2 \leq \sigma \leq 1 \\ f_\sigma(1.0) + \frac{\sigma}{0.1}(f_\sigma(0.2) - f_\sigma(1.0)) & 0 \leq \sigma < 0.1 \\ f_\sigma(0.2) & 0.1 \leq \sigma < 0.2 \end{cases} \tag{24}$$

Assuming the battery fade is 85% higher at 90% compared to 10% SOC [37], yields $k_{\sigma 2} = 0.769$. The battery is assumed to reach end of life after 10 years with 3000 cycles at 80% DOD with 50% average SOC and after 20 years with no cycling at 50% SOC. These assumptions yield $k_\delta = 3.092 \times 10^{-4}$ and $k_{\sigma 1} = 5.708 \times 10^{-6}$, respectively. The resulting SOC loss function and the corresponding linearized segments are shown in Fig. 3. The SOC loss curve is assumed to be flat between 10 and 20%,

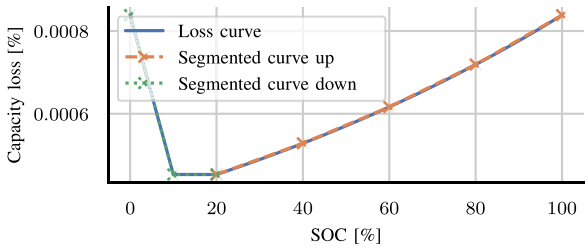

Fig. 3. Continuous and linearized SOC capacity loss functions.

Table 3
Overview of cases the proposed model has been tested on.

Case	Diesel generator [kW]	Battery [kWh]	Hydrogen [kWh]
1.	25	500	3300
2.	75	500	3300
3.	25	1000	–

Table 4
Overview of methods the proposed cases have been analyzed with.

Method	Forecast	DOD	SOC
a.	Perfect	X	X
b.	Deterministic		
c.	Stochastic		
d.	Stochastic	X	
e.	Stochastic		X
f.	Stochastic	X	X

and the SOC degradation is equal at 0 and 100% SOC to also capture capacity fade at low SOC.

3.3. Scenarios and stages

The time-series for wind and solar PV power and demand are based on actual values from the Rye MG through year 2020 and is available online [38]. The wind power has been scaled down to 60% of the original size. Wind, solar PV and demand have each been forecasted with a low, medium, and high scenario with probability 20, 60 and 20% respectively, based on the 0.2, 0.5, and 0.8 quantiles, yielding a combination of 27 scenarios. These have been ordered based on accumulated net production and reduced by selecting the median scenario of the percentiles 0–10, 10–30, 30–70, 70–90, and 90–100 with the corresponding probabilities 0.1, 0.2, 0.4, 0.2, and 0.1. More sophisticated scenario generation methods could have been used but are outside the scope of this paper. The individual percentiles are published online [39]. The interval between the four first stages are 6 h each, the next is 24 h, while the final is 72 h and repeated cyclically with discount factor 0.7 as described in Ref. [25]. The final stage is beyond the meterological forecast, and historical daily mean values are applied as scenarios using the same quantiles as previous stages.

3.4. Cases

The model has been simulated with three different variants of the system with respect to generator and EES sizes as shown in Table 3. The systems in cases *1* and *3* are energy constrained since the diesel generator is too small to meet the peak demand, hence load shedding depends on how the EESs are scheduled. However, the diesel generator in case *2* is large enough to always meet the peak demand, hence there is never a risk of scarcity unless the generator fails.

Each case will be analyzed with perfect forecast, deterministic forecast, and stochastic optimization, both with and without degradation in the optimization model as shown in Table 4.

4. Results and discussion

The main objective is to always meet the demand in the most cost effective way by using as much VRES generation as possible, and only using diesel if necessary to avoid load shedding. EES must also be utilized to maximize the VRES utilization and to minimize the diesel consumption and the load shedding. However, the battery degradation is a complicating element. Although cycling the battery is less expensive than generating power from the diesel generator, even for deep cycles, it is difficult due to the uncertainty in determining if the power charged now is needed later or if it can be consumed directly from VRES generation. It is therefore necessary to balance the cost of cycling the battery toward the expected diesel generation reduction. Additionally, there is an increasing cost associated with staying at high SOC. It can therefore be cost effective to keep the SOC low in periods with a stable high VRES generation to extend the battery's lifetime.

The results in Table 5 show that accounting for DOD and SOC degradation increases the load shedding in the cases *1* and *3*, and the diesel cost for all cases. However, the reduction in degradation surpasses the increase in diesel and load shedding costs and indicates an increase in expected battery life time of more than four years for all the cases when comparing methods *c* and *f*. A very common way to reduce battery degradation is to apply fixed operating limits, such as enforcing a permanent operating range between 10 and 90%. However, in situations where the only alternative is load shedding, it is optimal to utilize the full battery range since the cost reduction associated with reducing load shedding outperforms the cost accrued by degradation. The energy balance in the cases *1* and *2* show that the hydrogen system replaces some of the battery cycling from method *c* to *f*, since it has no degradation costs. However, case *3*, which has no hydrogen in the system, also shows a significant cost reduction associated with battery degradation when hydrogen is taken out of the system. SOC degradation without DOD degradation (method *e*) causes significant cycling and energy dumping through simultaneous charging and discharging of the battery, hence the DOD degradation reduces the occurrence of simultaneous charging and discharging caused by SOC degradation as indicated in method *f*.

Fig. 4a shows that the hydrogen SOC on average is lower when including the DOD degradation in methods *d* and *f*. The wind turbine peak capacity is 135 kW while the electrolyzer charge capacity is only 55 kW. In periods with very high wind power, the battery can act as a buffer for the hydrogen system that is unable to absorb the wind power peaks. However, DOD degradation makes this less profitable, resulting in lower hydrogen filling.

Fig. 4b shows that the battery SOC for methods *e* and *f*, where SOC degradation is included, is stable low in mid-year when the demand is low. These periods require relatively low stored energy to secure the supply, especially when the solar PV is delivering substantial energy due to many hours of sunlight through the summer. However, SOC degradation will, in general, lower the battery SOC, and DOD degradation will lower the hydrogen SOC, which in turn increases the risk of scarcity. The results in Table 5 shows a modest increase in both load shedding and diesel consumption when accounting for battery degradation.

5. Conclusions

Battery degradation is strongly connected to the operational pattern. In this study, the expected battery lifetime was prolonged by more than four years by properly accounting for degradation effects caused by DOD and SOC. Moreover, the total operating costs were reduced by up to 25% compared to the naive stochastic model without representation of degradation. However, battery degradation minimization also influences the operational pattern for the remaining resources in the system. The operational costs for generators and other EES technologies can, in the worst case scenario, increase even more than the savings

Table 5
Overview of operating costs, degradation costs, battery expected lifetime, VRES generation and EES charge/discharge for cases in Table 3 and methods in Table 4.

Case	Method	Operating cost [€]			Degradation cost [€]			[year]	Energy [MWh]		
		Total	Load shedding	Diesel	DOD	SOC up	SOC down	Lifetime	VRES	H2 ch/dch	Batt ch/dch
1	a	3719.7	0.00	3076	514	117	12	21.68	185.03	61.52/20.19	39.83/36.90
1	b	8541.1	4054.93	2840	1041	435	171	17.81	171.41	40.74/13.54	49.34/45.67
1	c	6011.1	968.94	2860	1328	731	123	16.26	166.73	32.87/11.02	52.67/48.73
1	d	5579.5	1086.00	2934	627	882	50	18.09	181.56	57.16/18.79	40.84/37.83
1	e	5804.1	1108.53	2861	1488	310	37	17.23	181.25	53.03/17.47	63.36/58.58
1	f	5256.8	1414.40	2964	582	268	29	20.62	183.48	60.64/19.90	39.71/36.79
2	a	3719.7	0.00	3076	514	117	12	21.68	185.03	61.52/20.19	39.83/36.90
2	b	4508.7	0.00	2917	998	445	149	17.98	171.41	40.86/13.58	47.87/44.31
2	c	5093.3	0.00	2864	1285	723	220	16.13	166.46	32.50/10.90	50.46/46.69
2	d	4575.3	0.00	2892	650	848	185	17.69	181.75	56.55/18.60	40.43/37.45
2	e	4704.9	0.00	2883	1494	313	16	17.27	181.26	53.10/17.49	62.37/57.63
2	f	3814.1	0.00	3000	556	253	6	20.90	183.46	60.79/19.95	38.50/35.63
3	a	4631.9	0.00	3459	771	348	53	19.45	141.21	–/–	56.93/52.66
3	b	9718.3	3822.67	3071	1228	1258	338	14.72	143.96	–/–	63.49/58.71
3	c	7202.8	775.38	3064	1436	1741	186	13.64	143.42	–/–	59.47/55.00
3	d	6968.8	1061.56	3091	885	1745	186	14.74	143.05	–/–	59.03/54.59
3	e	8467.5	1107.20	3215	3133	945	67	12.32	161.68	–/–	181.47/167.43
3	f	6188.1	1236.83	3321	776	789	66	17.86	140.56	–/–	56.43/52.20

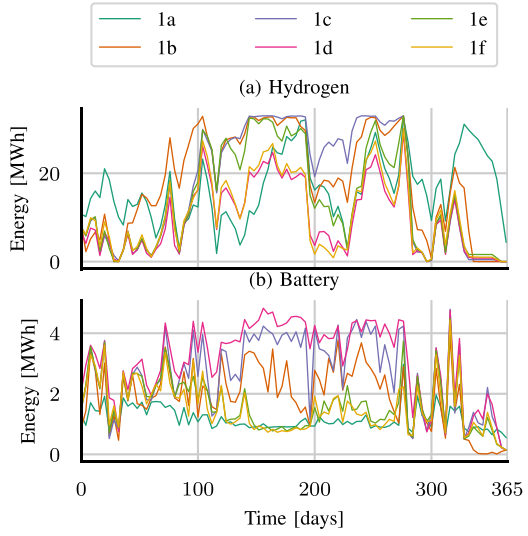

Fig. 4. Four day average SOC for case *1*.

for battery degradation. Degradation costs and inefficiencies associated with the operational pattern should therefore be considered for the whole system.

Dedicated battery degradation minimization can be contradictory to maximizing the security of supply, and the risk of scarcity must be balanced against the potential reduction in degradation. Realistic uncertainty models are therefore highly important.

The optimal operation of the future power system will to a greater extent be influenced by technology prices rather than fuel price, and energy adequacy rather than power adequacy. Future research should therefore give more attention to both the degradation of all the flexible resources in the system as well as precise uncertainty modeling to capture the future risk of scarcity accurately.

CRediT authorship contribution statement

Per Aaslid: Conceptualization, Methodology, Software, Formal analysis, Investigation, Visualization, Writing – original draft. **Magnus Korpås:** Conceptualization, Writing – review & editing. **Michael M. Belsnes:** Writing – review & editing, Project administration. **Olav B. Fosso:** Writing – review & editing, Supervision.

Declaration of competing interest

The authors declare that they have no known competing financial interests or personal relationships that could have appeared to influence the work reported in this paper.

References

[1] J. Geske, R. Green, Optimal storage, investment and management under uncertainty: It is costly to avoid outages! Energy J. 41 (2) (2020).
[2] P. Aaslid, M. Korpås, M.M. Belsnes, O.B. Fosso, Pricing electricity in constrained networks dominated by stochastic renewable generation and electric energy storage, Electr. Power Syst. Res. 197 (2021) 107169.
[3] H. Klinge Jacobsen, S.T. Schröder, Curtailment of renewable generation: Economic optimality and incentives, Energy Policy 49 (2012) 663–675.
[4] N.A. Sepulveda, J.D. Jenkins, A. Edington, D.S. Mallapragada, R.K. Lester, The design space for long-duration energy storage in decarbonized power systems, Nature Energy 6 (5) (2021) 506–516, 2021 6:5.
[5] M.A. Pellow, C.J. Emmott, C.J. Barnhart, S.M. Benson, Hydrogen or batteries for grid storage? A net energy analysis, Energy Environ. Sci. 8 (7) (2015) 1938–1952.
[6] P. Ahmadi, S.H. Torabi, H. Afsaneh, Y. Sadegheih, H. Ganjehsarabi, M. Ashjaee, The effects of driving patterns and PEM fuel cell degradation on the lifecycle assessment of hydrogen fuel cell vehicles, Int. J. Hydrogen Energy 45 (5) (2020) 3595–3608.
[7] B. Bidoggia, S.K. Kær, Estimation of membrane hydration status for standby proton exchange membrane fuel cell systems by complex impedance measurement: Constant temperature stack characterization, Int. J. Hydrogen Energy 38 (10) (2013) 4054–4066.
[8] J. Wang, H. Zhong, W. Tang, R. Rajagopal, Q. Xia, C. Kang, Y. Wang, Optimal bidding strategy for microgrids in joint energy and ancillary service markets considering flexible ramping products, Appl. Energy 205 (2017) 294–303.
[9] S. Wang, D. Guo, X. Han, L. Lu, K. Sun, W. Li, D.U. Sauer, M. Ouyang, Impact of battery degradation models on energy management of a grid-connected DC microgrid, Energy 207 (2020) 118228.
[10] H. Shuai, J. Fang, X. Ai, Y. Tang, J. Wen, H. He, Stochastic optimization of economic dispatch for microgrid based on approximate dynamic programming, IEEE Trans. Smart Grid 10 (3) (2019) 2440–2452.
[11] W. Gil-González, O.D. Montoya, E. Holguín, A. Garces, L.F. Grisales-Noreña, Economic dispatch of energy storage systems in dc microgrids employing a semidefinite programming model, J. Energy Storage 21 (2019) 1–8.
[12] M. Elkazaz, M. Sumner, D. Thomas, Energy management system for hybrid PV-wind-battery microgrid using convex programming, model predictive and rolling horizon predictive control with experimental validation, Int. J. Electr. Power Energy Syst. 115 (2020) 105483.
[13] T.A. Nguyen, M.L. Crow, Stochastic optimization of renewable-based microgrid operation incorporating battery operating cost, IEEE Trans. Power Syst. 31 (3) (2016) 2289–2296.
[14] D. Fioriti, D. Poli, P. Duenas-Martinez, I. Perez-Arriaga, Multi-year stochastic planning of off-grid microgrids subject to significant load growth uncertainty: overcoming single-year methodologies, Electr. Power Syst. Res. 194 (2021) 107053.
[15] W. Su, J. Wang, J. Roh, Stochastic energy scheduling in microgrids with intermittent renewable energy resources, IEEE Trans. Smart Grid 5 (4) (2014) 1876–1883.

[16] C. Ju, P. Wang, L. Goel, Y. Xu, A two-layer energy management system for microgrids with hybrid energy storage considering degradation costs, IEEE Trans. Smart Grid 9 (6) (2018) 6047–6057.
[17] M. Koller, T. Borsche, A. Ulbig, G. Andersson, Defining a degradation cost function for optimal control of a battery energy storage system, in: 2013 IEEE Grenoble Conference PowerTech, POWERTECH 2013, 2013.
[18] B. Xu, A. Oudalov, A. Ulbig, G. Andersson, D.S. Kirschen, Modeling of lithium-ion battery degradation for cell life assessment, IEEE Trans. Smart Grid 9 (2) (2018) 1131–1140.
[19] P. Aaslid, M. Korpås, M.M. Belsnes, O.B. Fosso, Stochastic optimization of microgrid operation with renewable generation and energy storages, IEEE Trans. Sustain. Energy 13 (3) (2022) 1481–1491.
[20] B. Xu, J. Zhao, T. Zheng, E. Litvinov, D.S. Kirschen, Factoring the cycle aging cost of batteries participating in electricity markets, IEEE Trans. Power Syst. 33 (2) (2018) 2248–2259.
[21] Remote EU project, 2021, [Online]. Available: https://www.remote-euproject.eu/remote-project/.
[22] P. Marocco, D. Ferrero, M. Gandiglio, M. Santarelli, Remote area energy supply with multiple options for integrated hydrogen-based technologies - deliverable number 2.2, 2018, [Online]. Available: https://www.remote-euproject.eu/remote18/rem18-cont/uploads/2019/03/REMOTE-D2.2.pdf.
[23] J.M. Maciejowski, Predictive Control with Constraints, Pearson Education, 2002.
[24] M.V.F. Pereira, L.M.V.G. Pinto, Multi-stage stochastic optimization applied to energy planning, Math. Program. 52 (1–3) (1991) 359–375.
[25] O. Dowson, The policy graph decomposition of multistage stochastic optimization problems, Networks 76 (1) (2020) 3–23.
[26] K. Linowsky, A.B. Philpott, On the convergence of sampling-based decomposition algorithms for multistage stochastic programs, J. Optim. Theory Appl. 125 (2) (2005) 349–366, 2005 125:2.
[27] J. Zou, S. Ahmed, X.A. Sun, Stochastic dual dynamic integer programming, Math. Program. (2018) 1–42.
[28] P. Keil, S.F. Schuster, J. Wilhelm, J. Travi, A. Hauser, R.C. Karl, A. Jossen, Calendar aging of lithium-ion batteries, J. Electrochem. Soc. 163 (9) (2016) A1872.
[29] K. Liu, T.R. Ashwin, X. Hu, M. Lucu, W.D. Widanage, An evaluation study of different modelling techniques for calendar ageing prediction of lithium-ion batteries, Renew. Sustain. Energy Rev. 131 (2020) 110017.
[30] J. Vetter, P. Novák, M.R. Wagner, C. Veit, K.C. Möller, J.O. Besenhard, M. Winter, M. Wohlfahrt-Mehrens, C. Vogler, A. Hammouche, Ageing mechanisms in lithium-ion batteries, J. Power Sources 147 (1–2) (2005) 269–281.
[31] Y. Gao, J. Jiang, C. Zhang, W. Zhang, Y. Jiang, Aging mechanisms under different state-of-charge ranges and the multi-indicators system of state-of-health for lithium-ion battery with Li(NiMnCo)o2 cathode, J. Power Sources 400 (2018) 641–651.
[32] J. Zhu, M. Knapp, D.R. Sø rensen, M. Heere, M.S. Darma, M. Müller, L. Mereacre, H. Dai, A. Senyshyn, X. Wei, H. Ehrenberg, Investigation of capacity fade for 18650-type lithium-ion batteries cycled in different state of charge (SoC) ranges, J. Power Sources 489 (2021) 229422.
[33] I. Laresgoiti, S. Käbitz, M. Ecker, D.U. Sauer, Modeling mechanical degradation in lithium ion batteries during cycling: Solid electrolyte interphase fracture, J. Power Sources 300 (2015) 112–122.
[34] C. Amzallag, J.P. Gerey, J.L. Robert, J. Bahuaud, Standardization of the rainflow counting method for fatigue analysis, Int. J. Fatigue 16 (4) (1994) 287–293.
[35] O. Dowson, L. Kapelevich, SDDP.jl: A julia package for stochastic dual dynamic programming, INFORMS J. Comput. 33 (1) (2021) 27–33.
[36] A. Millner, Modeling lithium ion battery degradation in electric vehicles, in: 2010 IEEE Conference on Innovative Technologies for An Efficient and Reliable Electricity Supply, CITRES 2010, 2010, pp. 349–356.
[37] D.I. Stroe, M. Swierczynski, A.I. Stroe, R. Teodorescu, R. Laerke, P.C. Kjaer, Degradation behaviour of lithium-ion batteries based on field measured frequency regulation mission profile, in: 2015 IEEE Energy Conversion Congress and Exposition, ECCE 2015, Institute of Electrical and Electronics Engineers Inc., 2015, pp. 14–21.
[38] TrønderEnergi, AI hackathon challenge - optimal control of microgrid, 2021, [Online]. Available: http://doi.org/10.5281/zenodo.5500209.
[39] P. Aaslid, Rye microgrid historical weather forecasts and stochastic scenarios [data set], 2021, [Online]. Available: https://doi.org/10.5281/zenodo.5526241.